

Comparative study of broadband electrodynamic properties of single-crystal and thin-film strontium titanate

A. T. Findikoglu,^{a)} Q. X. Jia, C. Kwon, D. W. Reagor, and G. Kaduchak
Materials Science and Technology Division, Los Alamos National Laboratory, Los Alamos,
New Mexico 87545

K. Ø. Rasmussen and A. R. Bishop
Theoretical Division, Los Alamos National Laboratory, Los Alamos, New Mexico 87545

(Received 16 September 1999; accepted for publication 1 November 1999)

We have used a coplanar waveguide structure to study broadband electrodynamic properties of single-crystal and thin-film strontium titanate. We have incorporated both time- and frequency-domain measurements to determine small-signal effective refractive index and loss tangent as functions of frequency (up to 4 GHz), dc bias (up to 10^6 V/m), and cryogenic temperature (17 and 60 K). The large-signal impulse response of the devices and the associated phenomenological nonlinear wave equation illustrate how dissipation and nonlinearity combine to produce the overall response in the large-signal regime. © 1999 American Institute of Physics. [S0003-6951(99)02952-6]

Strontium titanate (STO) is one of the most widely studied materials in condensed matter physics:¹ STO provided the prototype example for soft-phonon modes, for unusual electron/optical-phonon coupling leading to superconductivity, and for nonclassical exponents.² It was also the first material in which quantum paraelectricity was discovered.³ STO is also important from a technological point of view: its large dielectric constant and large dielectric breakdown field make it a potential candidate for storage capacitor cells in next-generation dynamic random access memories,⁴ and its large dielectric nonlinearity at cryogenic temperatures is a desirable property for various applications such as tunable filters and phased array antennas.^{5,6} Also, the synergistic compatibility between STO and high-temperature superconductor $\text{YBa}_2\text{Cu}_3\text{O}_{7-\delta}$ (YBCO) has recently led to an increased interest in their thin-film microwave applications.⁷ Although some marked differences in the electrodynamic properties of single-crystal and thin-film STO have been observed by several researchers,⁸ no detailed comparative study regarding their broadband microwave properties at cryogenic temperatures has yet been done.

In this letter, we report a comprehensive study of broadband electrodynamic properties of single-crystal and thin-film STO. By implementing a coplanar waveguide (CPW) geometry with identical YBCO electrode structures for both single-crystal and thin-film STO, we were able to make a direct comparison between them in terms of not only intrinsic electrodynamic characteristics but also practical implications. All films were pulsed-laser deposited. For this study, we have used three types of waveguides: single crystal, monolayer film, and bilayer film. All three devices have identical electrode structures, made from a $0.4\text{-}\mu\text{m}$ -thick epitaxial YBCO film, patterned in the form of a 7.8-cm -long meandering CPW with approximately a $20\text{-}\mu\text{m}$ -wide centerline, and a $15\text{-}\mu\text{m}$ -wide gap on $8\text{mm}\times 8\text{mm}$ templates. The

single-crystal sample uses, as nonlinear dielectric medium, a 1-mm -thick single-crystal STO (100) substrate (commercially available from K&R Creation) below the electrodes. The monolayer and bilayer samples use a $0.7\text{-}\mu\text{m}$ -thick epitaxial STO (100) film below the electrodes, and $0.7\text{-}\mu\text{m}$ -thick epitaxial STO films (100) below and above the electrodes, respectively, deposited on 0.5-mm -thick single-crystal LaAlO_3 (100) substrates. The details of film deposition and patterning were published previously.⁹

In the analysis of broadband characteristics of our CPWs, we have used an electrical circuit model based on lumped circuit equivalents of coupling impedance Z_c and input/output termination impedance Z_L for the external circuitry; and distributed CPW parameters of characteristic impedance Z , refractive index n , loss tangent $\tan \delta$, and waveguide length ℓ (see Fig. 1). We have used two types of lumped source; swept frequency (from 45 MHz to 4 GHz), and Gaussian-like impulse (pulse width ~ 0.05 ns for small signal, and 0.4 ns for large signal). In the case of swept-frequency measurements, the small-signal steady-state transmittance (e_T/e_I) is given by¹⁰

$$\frac{e_T(\omega)}{e_I(\omega)} = \frac{\left(\frac{2}{1 + \frac{Z_c}{Z_L}} \right) \left(\frac{1 + \frac{Z_c + Z_L - Z}{Z_c + Z_L + Z}}{e^{\gamma\ell} + \frac{Z_c + Z_L - Z}{Z_c + Z_L + Z} e^{-\gamma\ell}} \right)}{1 + \frac{(Z_L + Z_c)[Z_L + Z_c + Z \coth(\gamma\ell)]}{Z[(Z_L + Z_c)\coth(\gamma\ell) + Z]}} \quad (1)$$

where ω is the angular frequency. The complex propagation function γ is given by

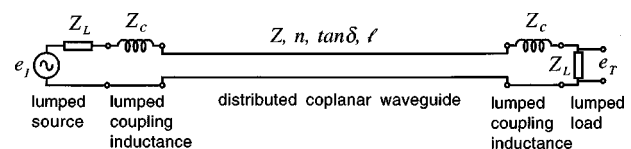


FIG. 1. Electrical circuit model.

^{a)}Electronic mail: findik@lanl.gov

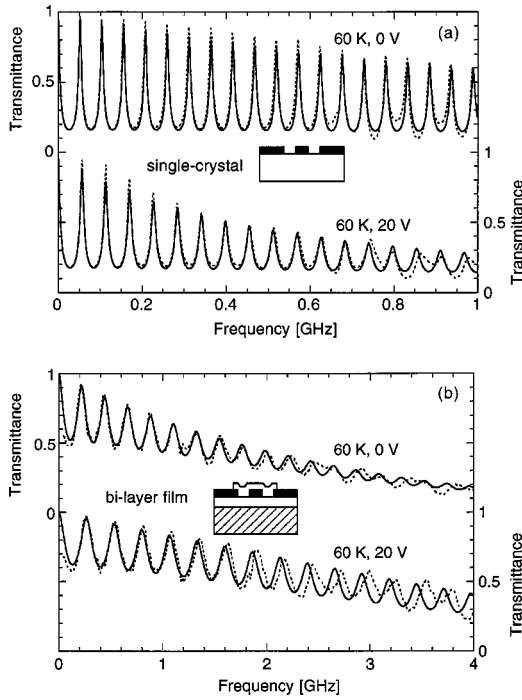


FIG. 2. Transmittance vs frequency at 60 K under 0 and 20 V bias for (a) single-crystal and (b) bilayer film samples (dashed lines are data, solid lines are fits; insets are schematic cross sections of waveguides).

$$\gamma = i\omega n/c + \frac{1}{2}\omega n \tan \delta/c, \quad (2)$$

where c is the speed of light in vacuum. Figure 2 shows fits to experimental data assuming purely inductive Z_c , and frequency-independent Z , Z_L , n , and $\tan \delta$. Basically, the separation of peaks (i.e., resonances), initial height of peaks, and decay of peaks with frequency are determined by n , Z , and $\tan \delta$, respectively. The bias is applied between the centerline and ground planes (20 V bias corresponds to $\sim 10^6$ V/m at the dielectric surface). Table I summarizes results of similar fits for all three waveguides at 17 and 60 K. To a good approximation, bias-dependent effects are quadratic for low voltages (< 2 V), and linear (shown in %) for high voltages (between 2 and 20 V). We note that $\tan \delta$ increases with bias in the single-crystal sample, whereas it decreases in the bilayer sample. Also, the bilayer sample shows noticeable dispersive (i.e., frequency-dependent) effects [see Fig. 2(b)].

To determine frequency-dependent effects quantitatively (and also to check the accuracy of swept-frequency fit results), we have used a Gaussian impulse generator as the source and performed a time-domain analysis.⁹ For the lowest-order impulse transmission (i.e., propagation length ℓ), the small-signal transmittance is given by⁹

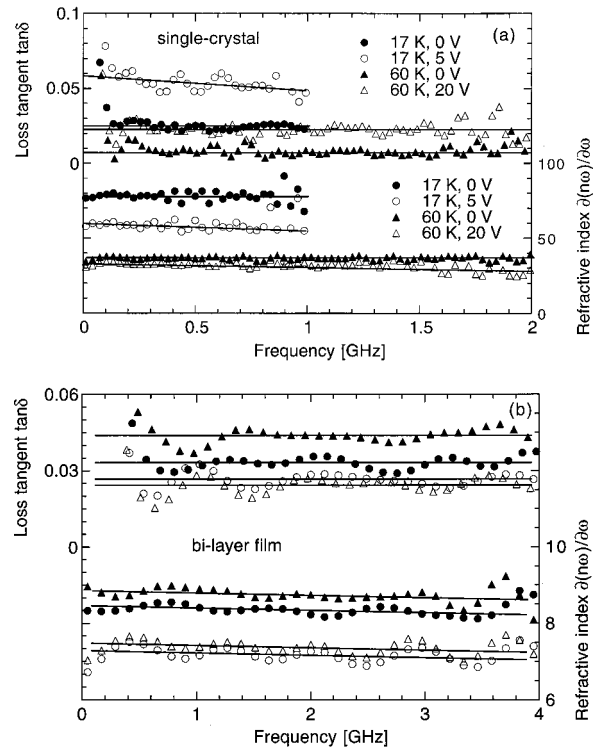


FIG. 3. Refractive index and loss tangent vs frequency at 17 and 60 K under 0, 5, and 20 V bias for (a) single-crystal and (b) bilayer film samples (symbols are data, solid lines are linear approximations).

$$\frac{e_T(\omega)}{e_I(\omega)} = \frac{8ZZ_L e^{-\gamma\ell}}{(Z + Z_L + Z_c)^2}. \quad (3)$$

By making certain assumptions and using Eqs. (2) and (3), we can readily obtain n and $\tan \delta$ as a function of frequency.⁹ Figure 3 shows results of such analysis for the single-crystal and bilayer film waveguides (the monolayer film waveguide had very similar characteristics to those of the bilayer film waveguide). The upperbound frequencies for the data were limited by the signal-to-noise ratio, and undulations in the data were caused by mutual inductance effects among parallel segments of the meandering lines of the waveguides. We note that frequency-dependent effects, such as reduction of n and $\tan \delta$ with frequency, become distinguishable with bias in the case of the single-crystal waveguide, especially at 17 K. However, such effects are virtually bias independent in the case of film waveguides. Also, at 60 K and 20 V bias, the bilayer film waveguide shows a much smaller refractive index but larger dielectric nonlinearity than, and similar effective loss tangent to, the single-crystal waveguide.

The ramifications of such bias-dependent small-signal

TABLE I. Sample type (Type), strontium titanate layer thickness (STO th.); broadband-frequency ($\sim 10^8$ – 10^9 Hz) averages for effective refractive index (n) and its fractional change per dc voltage bias ($\Delta n/\Delta Vn$), and effective loss tangent ($\tan \delta$) and its fractional change per dc voltage bias ($\Delta \tan \delta/\Delta V \tan \delta$) at 17 and 60 K.

Type	STO th. (μm)	n at 17 K	$\Delta n/\Delta Vn$ at 17 K (1/V)	$\tan \delta$ at 17 K	$\Delta \tan \delta/\Delta V \tan \delta$ at 17 K (1/V)	n at 60 K	$\Delta n/\Delta Vn$ at 60 K (1/V)	$\tan \delta$ at 60 K	$\Delta \tan \delta/\Delta V \tan \delta$ at 60 K (1/V)
Single crystal	1000	77.5	-5.0%	0.015	+30%	37.0	-0.4%	0.0035	+16%
Monolayer film	0.7	6.3	-0.5%	0.017	-2%	6.5	-0.4%	0.021	-2%
Bilayer film	0.7+0.7	8.3	-0.8%	0.027	-2%	8.8	-0.8%	0.033	-3%

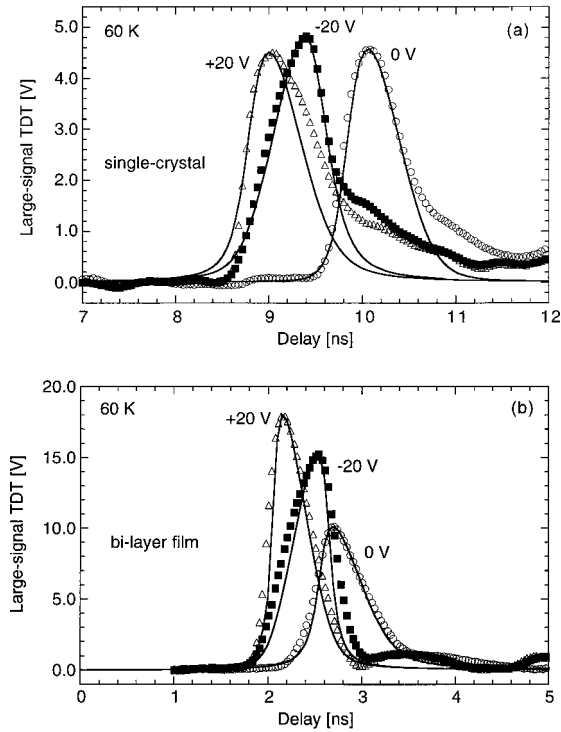


FIG. 4. Large-signal impulse transmission TDT at 60 K under 0, -20, and 20 V bias for (a) single-crystal and (b) bilayer film samples (symbols are data, lines are simulations).

characteristics for large-signal behavior are illustrated by Fig. 4. Here, the input is a 40 V Gaussian-like impulse with about a 0.4 ns pulse width for both devices. The transmitted impulse has a similar rise time and pulse shape (a shock-like front) for both waveguides at zero bias (the amplitudes are different due to impedance-mismatch effects). But under bias, the bilayer film CPW shows improved pulse-shaping effects due to reduced microwave loss, whereas the single-crystal CPW performance (dominated by combined effects of nonlinearity and loss) degrades due to increased loss. Such steep pulse fronts (or trailing edges) could be used, for example, for triggering. The solid lines are the results of simulations of the nonlinear wave equation

$$\frac{\partial v_s}{\partial t} + u(v_{dc} + v_s) \frac{\partial v_s}{\partial x} = \left(\alpha \frac{\partial}{\partial x} + \beta \frac{\partial^2}{\partial x^2} \right) H\{v_s\}, \quad (4)$$

where $H\{v_s\}$ denotes the Hilbert transform.⁹ This model, developed previously,⁹ has three basic components (all derived from the small-signal characteristics shown in Table I and Fig. 2): nonlinearity in the form of a voltage-dependent velocity $u(v_{dc} + v_s)$, where v_{dc} is the bias voltage and v_s is the signal voltage; frequency-dependent loss given by $\alpha \partial / \partial x H\{v_s\}$; and frequency-dependent refractive index given by $\beta \partial^2 / \partial x^2 H\{v_s\}$. Equation (4) only models the behavior of the signal in the interior of the device and does not account for nonlinear effects at the input and output terminals. Since the terminals are not impedance matched to the device, the exact influence of the terminals is not known for these large-amplitude signals. Consequently, we assume in the modeling that the terminals do not significantly change pulse shapes, but merely result in a simple amplitude scaling of the pulses. This scaling has been chosen in all cases such

that the simulation results match the amplitude of the experimental results. Our simulations also assume that the input pulse is an ideal Gaussian impulse, whereas the experimental pulse is slightly asymmetric and has a shoulder at the trailing edge.

The decrease of n with bias in both single crystals and thin films is well described by essentially “hardening” of soft phonons (n in films is reduced and has different temperature dependence, most likely due to increased stress and defect density in the films).¹¹ Recently, Vendik, Ter-Martirosyan, and Zubko¹² revised a model first used by Bethe¹³ to describe microwave losses in incipient ferroelectrics. According to this model, losses due to scattering of phonons by residual/localized ferroelectric polarization is likely to be dominant in single crystals, since this mechanism predicts the experimentally observed increase of loss with both decreasing temperature and increasing bias. For films, the experimental observation of weak temperature dependence and reduction with bias of loss is consistent with a loss mechanism based on transformation of microwave photons into acoustic oscillations at charged defects. However, the fact that this model for all mechanisms predicts linearly increasing $\tan \delta$ with frequency (for single-crystal STO at 140 K, such linear dependence has been experimentally observed),¹⁴ while we observe essentially frequency-independent $\tan \delta$ for all devices ≤ 60 K, means that an improved model is needed—for example, one that takes strong-correlation effects with the lattice into account.^{9,15} We have no definitive explanation for the small dispersive effects we have seen, except to note that monolayer and bilayer films showed very similar dispersion (i.e., dispersion is unlikely to be caused by inhomogeneity of the dielectric medium in the CPW structure). Finally, as demonstrated by Table I and Figs. 2–4, typical thin-film STO could offer superior performance to single-crystal STO for some tunable device applications—clearly, the manifest definition of performance would depend critically on the specific application.

- ¹R. A. Cowley, *Philos. Trans. R. Soc. London, Ser. A* **354**, 2799 (1996).
- ²R. Vacher, J. Pelous, B. Hennion, G. Coddens, E. Cortens, and K. A. Muller, *Europhys. Lett.* **17**, 45 (1992).
- ³K. A. Muller and H. Burkard, *Phys. Rev. B* **19**, 3593 (1979).
- ⁴P. Y. Lesaichere, H. Yamaguchi, Y. Miyasaka, H. Watanabe, H. Ono, and M. Yoshida, *Integr. Ferroelectr.* **8**, 201 (1995).
- ⁵A. T. Findikoglu, Q. X. Jia, X. D. Wu, G. J. Chen, T. Venkatesan, and D. W. Reagor, *Appl. Phys. Lett.* **68**, 1651 (1996).
- ⁶F. A. Miranda, R. R. Romanofsky, F. W. VanKeuls, C. H. Mueller, R. E. Treece, and T. V. Rivkin, *Integr. Ferroelectr.* **17**, 231 (1997).
- ⁷M. J. Lancaster, J. Powell, and A. Porch, *Supercond. Sci. Technol.* **11**, 1323 (1998).
- ⁸See, for example, S. Gevorgian, E. Carlsson, S. Rudner, L. D. Wernlund, X. Wang, and U. Helmerson, *IEEE Proc., Part H: Microwaves, Antennas Propag.* **143**, 397 (1996); H. C. Li, W. D. Si, A. D. West, and X. X. Xi, *Appl. Phys. Lett.* **73**, 190 (1998).
- ⁹A. T. Findikoglu, D. W. Reagor, K. O. Rasmussen, A. R. Bishop, N. Gronbech-Jensen, Q. X. Jia, Y. Fan, C. Kwon, and L. A. Ostrovsky, *J. Appl. Phys.* **86**, 1558 (1999).
- ¹⁰See, for example, K. E. Collin, *Foundations for Microwave Engineering* (McGraw-Hill, New York, 1992), pp. 71–96.
- ¹¹J. M. Worlock and P. A. Fleury, *Phys. Rev. Lett.* **19**, 1176 (1967).
- ¹²O. G. Vendik, L. T. Ter-Martirosyan, and S. P. Zubko, *J. Appl. Phys.* **84**, 993 (1998).
- ¹³K. Bethe, *Philips Res. Rep.* **2**, 1 (1970).
- ¹⁴V. L. Gurevich and A. K. Tagantsev, *Adv. Phys.* **40**, 719 (1991).
- ¹⁵R. M. Hill and A. K. Jonscher, *Contemp. Phys.* **24**, 75 (1984).